Impact of CT attenuation correction method on quantitative respiratory-correlated (4D) PET/CT imaging

Matthew J. Nyflot[a)]
Department of Radiation Oncology, University of Washington, Seattle, Washington 98195-6043

Tzu-Cheng Lee
Department of Bioengineering, University of Washington, Seattle, Washington 98195-6043

Adam M. Alessio
Department of Radiology, University of Washington, Seattle, Washington 98195-6043

Scott D. Wollenweber and Charles W. Stearns
GE Healthcare, Waukesha, Wisconsin 53188

Stephen R. Bowen
Department of Radiation Oncology, University of Washington, Seattle, Washington 98195-6043
and Department of Radiology, University of Washington, Seattle, Washington 98195-6043

Paul E. Kinahan
Department of Radiology, University of Washington, Seattle, Washington 98195-6043

Purpose: Respiratory-correlated positron emission tomography (PET/CT) 4D PET/CT is used to mitigate errors from respiratory motion; however, the optimal CT attenuation correction (CTAC) method for 4D PET/CT is unknown. The authors performed a phantom study to evaluate the quantitative performance of CTAC methods for 4D PET/CT in the ground truth setting.

Methods: A programmable respiratory motion phantom with a custom movable insert designed to emulate a lung lesion and lung tissue was used for this study. The insert was driven by one of five waveforms: two sinusoidal waveforms or three patient-specific respiratory waveforms. 3DPET and 4DPET images of the phantom under motion were acquired and reconstructed with six CTAC methods: helical breath-hold (3DHEL), helical free-breathing (3DMOT), 4D phase-averaged (4DAVG), 4D maximum intensity projection (4DMIP), 4D phase-matched (4DMATCH), and 4D end-exhale (4DEXH) CTAC. Recovery of SUV_{max}, SUV_{mean}, SUV_{peak}, and segmented tumor volume was evaluated as RC_{max}, RC_{mean}, RC_{peak}, and RC_{vol}, representing percent difference relative to the static ground truth case. Paired Wilcoxon tests and Kruskal–Wallis ANOVA were used to test for significant differences.

Results: For 4DPET imaging, the maximum intensity projection CTAC produced significantly more accurate recovery coefficients than all other CTAC methods ($p < 0.0001$ over all metrics). Over all motion waveforms, ratios of 4DMIP CTAC recovery were 0.2 ± 5.4, -1.8 ± 6.5, -3.2 ± 5.0, and 3.0 ± 5.9 for RC_{max}, RC_{peak}, RC_{mean}, and RC_{vol}. In comparison, recovery coefficients for phase-matched CTAC were -8.4 ± 5.3, -10.5 ± 6.2, -7.6 ± 5.0, and -13.0 ± 7.7 for RC_{max}, RC_{peak}, RC_{mean}, and RC_{vol}. When testing differences between phases over all CTAC methods and waveforms, end-exhale phases were significantly more accurate ($p = 0.005$). However, these differences were driven by the patient-specific respiratory waveforms; when testing patient and sinusoidal waveforms separately, patient waveforms were significantly different between phases ($p < 0.0001$) while the sinusoidal waveforms were not significantly different ($p = 0.98$). When considering only the subset of 4DMATCH images that corresponded to the end-exhale image phase, 4DEXH, mean and interquartile range were similar to 4DMATCH but variability was considerably reduced.

Conclusions: Comparative advantages in accuracy and precision of SUV metrics and segmented volumes were demonstrated with the use of the maximum intensity projection and end-exhale CT attenuation correction. While respiratory phase-matched CTAC should in theory provide optimal corrections, image artifacts and differences in implementation of 4DCT and 4DPET sorting can degrade the benefit of this approach. These results may be useful to guide the implementation, analysis, and development of respiratory-correlated thoracic PET/CT in the radiation oncology and diagnostic settings. © 2015 American Association of Physicists in Medicine. [http://dx.doi.org/10.1118/1.4903282]

1. INTRODUCTION

Positron emission tomography (PET) with ^{18}F-fluorodeoxy-glucose (FDG) is commonly used in the management of patients with lung cancer and is of considerable interest in quantitative imaging of the thorax. The addition of PET imaging is useful in staging of atelectasis and the mediastinal nodes.[1–3] The use of PET-guided segmentation may reduce interobserver variability compared to CT-only-guided segmentation and provide clinical benefit for radiotherapy target definition.[4–7] FDG metrics have been shown to predict therapeutic outcome early in the course of chemoradiotherapy in nonsmall cell lung cancer.[8–10] Radiation dose escalation to metabolically active tumor subvolumes, so-called "dose painting," has been proposed as a strategy to increase tumor control.[11,12]

Mismatch of PET data with computed tomography attenuation correction (CTAC) due to respiratory motion is a known source of quantitative error in PET imaging.[13–19] In theory, this can be corrected by matching individual PET and CT phases which have been generated by respiratory-correlated PET (4DPET)[20] and respiratory-correlated CT (4DCT).[21–24] However, differences in the physics of image acquisition between PET and fast CT imaging lead to challenges for this approach. Namely, emission PET integrates motion over several minutes with large (i.e., 15 cm) axial fields-of-view, while fast helical or axial transmission CT has the effect of "freezing" motion over several seconds with smaller (i.e., 2 cm) axial fields-of-view. In practice, both imaging modalities are known to be susceptible to respiratory imaging artifacts. Therefore, it is important to understand the quantitative impact of CTAC methods for respiratory-correlated PET imaging.

A small body of prior work exists regarding choice of CTAC method for 4DPET quantification in the ground truth setting with anthropomorphic phantoms. Nagel *et al.* found 4DPET with phase-matched 4DCT attenuation correction was superior to 3DPET with helical CT attenuation correction under sinusoidal respiratory motion.[25] Ponisch *et al.* and Park *et al.* investigated 4DPET with phase-matched 4DCTAC and 4DPET with helical CTAC under sinusoidal motion and found superior recovery with phase-matched 4DCTAC.[26,27] Killoran *et al.* investigated artifacts at the lung–diaphragm interface with helical CTAC, phase-averaged 4DCT, and phase-matched 4DCT attenuation correction under sinusoidal motion.[28] They noted minor improvements in quantification with phase-matched 4DCTAC versus phase-averaged 4DCTAC or helical CTAC in regions with lung-equivalent background density, but no advantage to using phase-matched 4DCTAC at interfaces of similar tissue density.

We present new work to comprehensively evaluate the accuracy of six CTAC methods for 4DPET imaging using measured data from a respiratory phantom. We report on 4DCT maximum intensity projection (4DMIP) attenuation correction, which has shown advantages in accuracy of cardiac PET (Ref. 29) but has not been previously investigated in thoracic PET. While prior phantom studies considered only sinusoidal motion cases, we investigate patient-specific respiratory waveforms, which more accurately represent clinical conditions and may be expected to increase CT and PET mismatch due to irregular respiratory patterns. Additionally, we report on the recovery of metrics not previously investigated, including SUV_{peak}, which is recommended over SUV_{max} by PERCIST guidelines,[30] and SUV_{mean}, which is commonly used in the literature. Finally, comparisons of accuracy between 3D and 4D PET are evaluated in context of CTAC method. These results may be useful to guide the implementation, analysis, and development of respiratory-correlated thoracic PET/CT in the radiation oncology and diagnostic settings.

2. METHODS

2.A. Phantom design

A programmable respiratory motion phantom consisting of the Quasar™ Multipurpose Torso Phantom and Respiratory Motion Assembly (Modus Medical Devices, Inc., London, ON) was used for this study (Fig. 1). A custom movable insert was designed to emulate a lung lesion (2.2 cm fillable NEMA sphere) and lung tissue (fillable chamber with polystyrene beads to mimic lung tissue density). A static control insert was similarly designed with a 3.7 cm NEMA sphere and fillable chamber with polystyrene beads. Phantom spheres and lung-equivalent backgrounds were filled with ^{18}F-FDG solutions at nominal activity concentrations of 1.0 and 0.125 MBq/ml, respectively.

The moving insert was driven by one of the five waveforms: two sinusoidal waveforms or three patient-specific respiratory waveforms. The sinusoidal waveforms had 1.5 and 3.0 cm peak-to-peak amplitude and 4 s period. The patient-specific
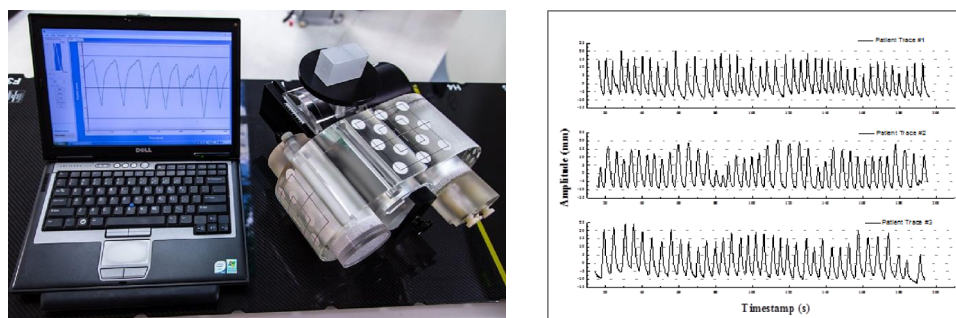
FIG. 1. Left: programmable respiratory phantom with custom anthropomorphic PET inserts. Right: patient-specific respiratory waveforms under investigation, representing regular, irregular, and intermediate respiratory waveforms. Two sinusoidal waveforms were also investigated.

waveforms were supplied by the vendor and had the following parameters as depicted in Fig. 1: 3.0 cm peak-to-peak amplitude; mean amplitude 1.86 ± 0.27, 2.00 ± 0.42, and 2.16 ± 0.31 cm; mean period 4.2 ± 0.7, 4.5 ± 0.7, 4.9 ± 0.7 s, respectively. The Quasar phantom drives a platform which is suitable for mounting a real-time position management (RPM) marker (Varian Medical Systems, Palo Alto, CA). While surrogacy between motion of the RPM marker (i.e., the chest wall) and tumor motion can be a source of error in patient imaging, with the phantom this motion is mechanically coupled. As a result, the motion tracking is only limited by the optical performance of the system.

2.B. Image acquisition and reconstruction

PET/CT images were acquired on a Discovery STE PET/CT scanner (GE Healthcare, Waukesha, WI) at a single 15 cm axial field of view in 3D mode. PET emission data were acquired for 5 min under the no-motion condition to define the reference case. Then, PET data were acquired under the five motion conditions with matched numbers of emission coincidence counts to the reference case (261.5×10^6 events; typical whole-body FDG fully 3D PET acquisitions acquire $200–300 \times 10^6$ prompt events for each bed position). Phantom motion waveforms were captured in real-time with the RPM infrared camera system. PET emission data were in-line tagged at peak inspiration during list mode acquisition to enable 4D data sorting.

Following PET acquisition, CT images were acquired. A static helical CT (3DHEL) analogous to an idealized breath-hold CT was used as the reference CTAC dataset. Then, CT images were acquired for each respiratory waveform, including a helical CT under respiratory motion (3DMOT) analogous to a free-breathing CT and a cine CT series for 4DCT reconstruction. For 4DCT acquisitions, the cine duration parameter was defined as the breathing period plus 1 s and the time between cine images parameter was defined as the respiratory period in seconds divided by 10. All CT imaging was acquired with $512 \times 512 \times 176$ voxels, $0.0977 \times 0.0977 \times 0.25$ cm/voxel at 120 kV and auto mAs.

For 4DCT reconstruction, RPM traces were visually reviewed for accuracy of peak fitting retrospectively in the RPM software. RPM traces were used to phase-define the cine CT data in Advantage 4D (GE Healthcare). Five 4DCT phase-defined images were selected with 10% phase shift for

phase-matched CTAC reconstruction (4DMATCH) so that 4DCT phases would be centered on 4DPET phases in the respiratory cycle (Fig. 2). Additionally, 4DCT phase-binned images were reformatted into average intensity projection (4DAVG) and maximum intensity projection (4DMIP) CT images, and the 4DCT phase image that corresponded to the end-exhale phase was identified as 4DEXH. The protocols are summarized in Table I.

CT data were then transferred from the Advantage workstation to the PET/CT console for attenuation correction of PET data. The static PET with static helical CTAC was used to define the reference case. For the five motion cases, all PET data were reconstructed in both 3D mode and 4D mode with five equal phase bins unlisted from the tagged emission data (Fig. 2). The choice of five phase bins was based on Park *et al.*, who found 5 bins to provide superior image quantification versus 10 or 20 bins,[27] in addition to the clinical practicality of this approach. CT attenuation correction was applied to both the 3D and to each phase of the 4D PET data with 3DHEL, 3DMOT, 4DAVG, 4DMIP, and 4DMATCH CTAC methods, and to the end-exhale phase of the 4DPET data with 4DEXH (Fig. 3). For the 4DMATCH reconstruction, visual inspection of image phases was required to assure optimal matching between 4DPET and 4DCT images (i.e., PET bin 1 might best match the CT bin located between 10% and 30% phase or 90%–10% phase). Note that in our naming convention, 3DPET refers to non-respiratory-correlated PET in 3D mode, 4DPET refers to respiratory-correlated PET, 3DCT refers to non-respiratory-correlated helical CT, and 4DCT refers to respiratory-correlated cine CT.

In total, 24 3DPET and 125 4DPET images were reconstructed over all motion cases. All PET images were reconstructed with an ordered-subsets-expectation–maximization (OSEM) algorithm (4 iterations, 28 subsets) using $128 \times 128 \times 47$ voxels, $0.547 \times 0.547 \times 0.327$ cm/voxel, 0.8 cm full-width at half-maximum filtration, and standard Z filtering.

2.C. Image analysis

Quantitative accuracy was evaluated with ratios between the motion case and the reference case for the following metrics: SUV_{max}, SUV_{peak}, SUV_{mean}, and fixed threshold volume segmentation. Two reference methods were defined. In reference method I, activity of the 2.2 cm sphere under respiratory motion was compared to the activity measured from the
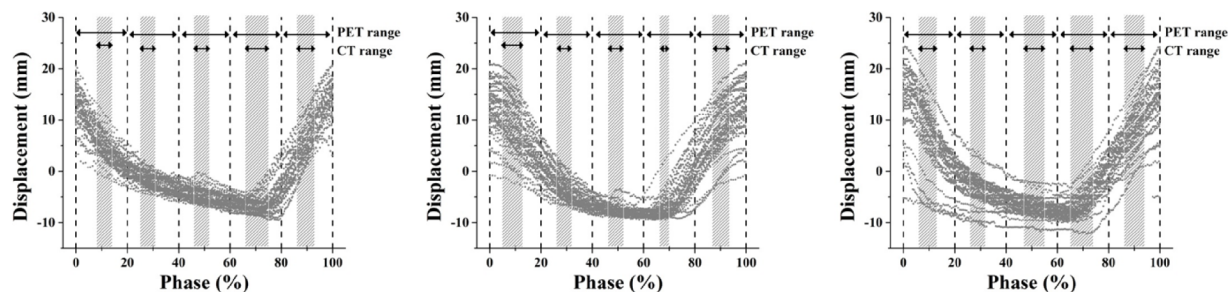
Fig. 2. Schematic representation of 4DPET and 4DCT phase range versus phantom displacement for each of the patient-specific respiratory waveforms. Phase range for the 4DCT is depicted with the gray shading and centered within PET bins. Phase range for the 4DPET is depicted with vertical dashed lines.

TABLE I. Summary of investigated PET and CTAC methods.

PET	PET acquired under motion?	CTAC	CTAC acquired under motion?	Description
3DPET	No	3DHEL	No	Motion-free 3DPET with motion-free helical CTAC (reference case)
3DPET	Yes	3DHEL	No	3DPET with motion-free helical CTAC (representing idealized breath hold)
3DPET	Yes	3DMOT	Yes	3DPET with helical CTAC (representing free-breathing helical CT)
3DPET	Yes	4DAVG	Yes	3DPET with average intensity projection 4DCTAC
3DPET	Yes	4DMIP	Yes	3DPET with maximum intensity projection 4DCTAC
4DPET	Yes	3DHEL	No	4DPET with motion-free helical CTAC (representing idealized breath hold)
4DPET	Yes	3DMOT	Yes	4DPET with helical CTAC (representing free-breathing helical CT)
4DPET	Yes	4DAVG	Yes	4DPET with average intensity projection 4DCTAC
4DPET	Yes	4DMIP	Yes	4DPET with maximum intensity projection 4DCTAC
4DPET	Yes	4DMATCH	Yes	4DPET with phase-matched 4DCTAC
4DPET	Yes	4DEXH	Yes	End-exhale phase 4DPET with end-exhale phase 4DCTAC

2.2 cm sphere in the static reference scan. For method II, activity of the 2.2 cm sphere under respiratory motion was normalized to the activity of the static 3.7 cm sphere in the same scan. Results reported are for method I unless otherwise indicated and a comparison of reference methods is shown in Appendix.

Activity and volume recovery coefficients, defined as the ratio of uptake or segmented volume between the moving sphere and the reference sphere, were calculated. Change in recovery coefficients of maximum, mean, and peak activity and segmented volume was defined as RC_{max}, RC_{peak}, RC_{mean}, and RC_{vol}; for example, RC_{max} was defined as the ratio of the voxel with maximum activity in the moving sphere divided by the voxel with maximum activity in the reference sphere minus 1. The lesion volume of interest was formed by threshold segmentation (Fig. 4). The reference segmentation threshold was defined on the no-motion reference PET image to correspond to the internal volume of the 2.2 cm diameter sphere. The threshold (320 kBq/mL) corresponded to 45.5% of maximum activity. To test the impact of threshold choice on segmentation results, threshold segmentation with 10% change in threshold setting to 40.5% and 49.5% was also investigated, which is in line with prior phantom studies.[31,32]

The segmentation thresholds were subsequently applied to the cases under motion following decay correction. RC_{peak} was defined as the ratio of the mean activity of a 1 cm diameter sphere that is placed such that it encompasses the greatest integral activity in the respective images. RC_{mean} was defined as the ratio of mean uptake in the reference threshold segmentation volumes defined above. For 4DPET analysis, recovery coefficients were averaged across all phase bins unless explicitly noted.

To investigate effects of CTAC on the low-activity background region surrounding the lesion, a 2 cm isotropic expansion was performed around the reference segmentation volume on the static scan. Then, the segmented lesion volume on each scan was subtracted from this expansion to form a background volume of interest for each scan (Fig. 4). Ratios of activity between the motion case and the static reference case were evaluated.

Image analysis was done in MIM v.6.2.5 (MIM Software, Inc., Cleveland, OH). To ensure robustness against nonnormal distributions, statistical testing was performed with nonparametric paired Wilcoxon tests. To correct for the effect of multiple sampling with repeated hypothesis testing, Bonferroni's correction was applied such that the threshold
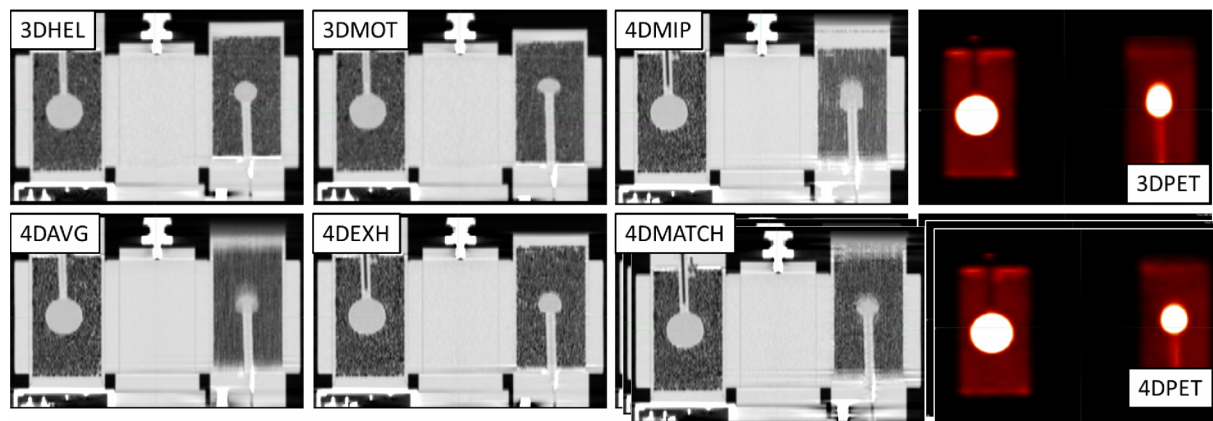
FIG. 3. Parameter space showing examples of all CTAC and PET acquisitions for a typical patient-specific respiratory waveform. 3DHEL: static helical "breath hold" CTAC. 3DMOT: helical "free-breathing" CTAC under motion. 4DMIP: 4D maximum intensity projection CTAC. 4DAVG: 4D average intensity projection CTAC. 4DEXH: 4D end-exhale phase CTAC. 4DMATCH: 4D phase-matched CTAC (one of five phases shown). 3D PET: non-respiratory-correlated PET. 4D PET: respiratory-correlated PET (one of five phases shown).
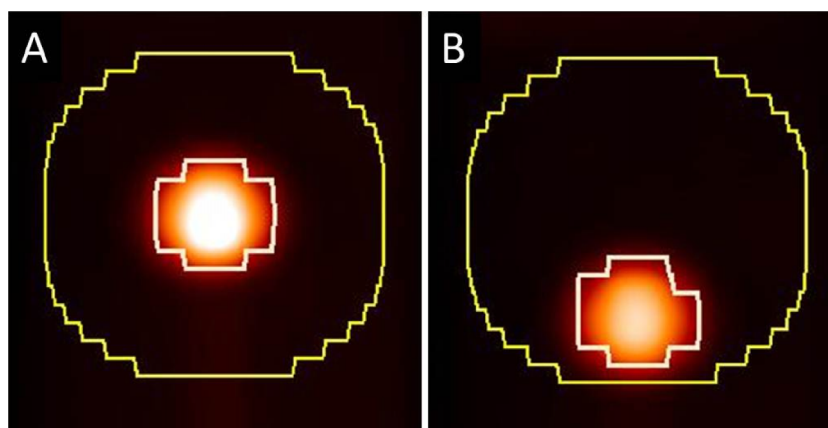
Fig. 4. Segmented volumes of interest in the reference case of no motion (A) and the case of 3.0 cm sinusoidal motion (B). The reference volume (left inner contour) was defined by taking the percent threshold segmentation that yielded the known object volume on the reference PET/CT. Then, the same percent threshold segmentation was applied to the object under motion (right inner contour). To investigate the effects of CTAC in the vicinity of the lesion, a 2 cm isotropic expansion was applied to the reference case (left outer contour) and the same contour was used for all motion cases (right outer contour).

of significance was set at $\alpha = 0.002$. To evaluate trends across multiple variables, nonparametric Kruskal–Wallis ANOVA was used.

3. RESULTS

Recovery of maximum, mean, and peak activity and segmented volume is shown as RC_{max}, RC_{peak}, RC_{mean}, and RC_{vol} in Tables II and III for patient-specific and sinusoidal motion, respectively. Perfect recovery of activity under motion relative to the reference case would result in percent difference of zero. Box plots of recovery for 4DPET results as a function of CTAC method and image metric are shown in Fig. 5.

3.A. 3D vs 4D PET

Activity and volume recovery were improved through the use of phase-binned (4D) PET versus nonbinned (3D) PET, especially for cases with large motion. In the worst case of the 3.0 cm peak-to-peak sinusoidal waveform with the

helical CTAC under motion (3DMOT), errors on the order of 40%–50% were observed (-40.8%, -41.9%, -23.2%, -52.1% for RC_{max}, RC_{peak}, RC_{mean}, and RC_{vol}, respectively). The best results for 3DPET reconstruction of the 3.0 cm peak-to-peak sinusoidal waveform were obtained with the 4DMIP CTAC, but errors on the order of 30%–40% persisted (-33.5%, -34.5%, -17.1%, -40.9%). For the 4DPET reconstruction, errors were reduced to 10%–15% for the 3DMOT CTAC case ($-9.0 \pm 3.0\%$, $-11.2 \pm 3.7\%$, $-8.1 \pm 2.8\%$, $-13.5 \pm 2.7\%$) and to less than 5% for the 4DMIP CTAC case ($2.3 \pm 2.3\%$, $-0.3 \pm 4.2\%$, $-2.3 \pm 3.9\%$, $3.1 \pm 3.0\%$). Smaller differences were measured between 3D and 4D PET under patient-specific motion and the 1.5 cm sinusoidal motion, on the order of 10% and 5%, respectively (Tables II and III).

3.B. Impact of CTAC on 4D PET

For 4DPET imaging, the maximum intensity projection (4DMIP) CTAC produced significantly more accurate recovery coefficients than all other CTAC methods ($p < 0.0001$ over all metrics; Fig. 5). Over all waveforms, ratios of 4DMIP

Table II. Percent difference of recovery of SUV and volume metrics as a function of PET reconstruction and CTAC under patient-specific respiratory motion versus the no-motion reference case (recovery coefficients and standard deviations are calculated across waveforms and image phases).

		Patient waveform 1, 2, and 3			
	CTAC	RC_{max} (%)	RC_{peak} (%)	RC_{mean} (%)	RC_{vol} (%)
3DPET	3DHEL	-15.5 ± 2.8	-18.5 ± 3.0	-14.1 ± 1.9	-19.2 ± 5.0
	3DMOT	-20.3 ± 3.2	-22.6 ± 3.1	-15.6 ± 0.7	-27.1 ± 7.9
	4DAVG	-15.8 ± 2.6	-18.6 ± 3.1	-14.5 ± 2.1	-17.9 ± 8.3
	4DMIP	-8.6 ± 2.7	-11.5 ± 3.2	-10.5 ± 2.0	-3.1 ± 3.5
4DPET	3DHEL	-9.9 ± 4.0	-12.6 ± 4.9	-10.1 ± 2.8	-11.2 ± 9.2
	3DMOT	-14.1 ± 3.3	-15.9 ± 4.2	-11.9 ± 2.2	-15.1 ± 8.9
	4DAVG	-10.6 ± 5.5	-12.8 ± 6.1	-9.8 ± 3.5	-12.9 ± 11.1
	4DMATCH	-12.3 ± 5.7	-14.5 ± 6.5	-10.6 ± 3.7	-16.4 ± 11.6
	4DEXH	-6.8 ± 4.3	-8.9 ± 3.6	-7.2 ± 2.8	-9.7 ± 4.2
	4DMIP	-2.4 ± 5.3	-4.7 ± 6.2	-5.0 ± 5.2	0.2 ± 5.0

TABLE III. Percent difference of recovery of SUV and volume metrics as a function of PET reconstruction and CTAC under sinusoidal respiratory motion versus the no-motion reference case (recovery coefficients and standard deviations are calculated across image phases).

1.5 cm sine wave

	CTAC	RC_{max} (%)	RC_{peak} (%)	RC_{mean} (%)	RC_{vol} (%)
3DPET	3DHEL	−7.7	−10.9	−10.1	−9.9
	3DMOT	−9.6	−13.4	−12.1	−10.5
	4DAVG	−8.5	−11.5	−9.8	−12.3
	4DMIP	−1.7	−4.9	−7.1	3.6
4DPET	3DHEL	−1.7 ± 1.0	−2.6 ± 0.9	−0.6 ± 1.1	−9.1 ± 1.9
	3DMOT	−4.3 ± 3.5	−4.7 ± 2.4	−2.1 ± 2.3	−10.1 ± 3.6
	4DAVG	−2.2 ± 1.4	−2.9 ± 1.3	−1.3 ± 1.3	−8.3 ± 1.2
	4DMATCH	−3.3 ± 0.6	−4.2 ± 1.2	−1.6 ± 1.0	−10.9 ± 5.4
	4DEXH	−4.1	−5.5	−1.5	−16.2
	4DMIP	5.7 ± 0.8	5.4 ± 1.2	1.0 ± 1.3	11.2 ± 1.8

3.0 cm sine wave

	CTAC	RC_{max} (%)	RC_{peak} (%)	RC_{mean} (%)	RC_{vol} (%)
3DPET	3DHEL	−38.0	−39.6	−22.6	−48.1
	3DMOT	−40.8	−41.9	−23.2	−52.1
	4DAVG	−40.0	−41.1	−24.4	−48.1
	4DMIP	−33.5	−34.5	−17.1	−40.9
4DPET	3DHEL	−8.0 ± 2.3	−10.4 ± 2.6	−8.6 ± 2.2	−9.9 ± 4.1
	3DMOT	−9.0 ± 3.0	−11.2 ± 3.1	−8.1 ± 2.8	−13.5 ± 2.7
	4DAVG	−9.0 ± 2.1	−11.2 ± 3.7	−8.8 ± 4.3	−11.4 ± 4.8
	4DMATCH	−6.3 ± 2.7	−9.1 ± 4.3	−6.7 ± 5.3	−12.1 ± 4.1
	4DEXH	−3.5	−3.9	−1.8	−8.3
	4DMIP	2.3 ± 2.3	−0.3 ± 4.2	−2.3 ± 3.9	3.1 ± 3.0

CTAC recovery were $0.2 ± 5.4$, $−1.8 ± 6.5$, $−3.2 ± 5.0$, and $3.0 ± 5.9$ for RC_{max}, RC_{peak}, RC_{mean}, and RC_{vol}. In comparison, recovery coefficients for phase-matched CTAC (4DMATCH) were $−8.4 ± 5.3$, $−10.5 ± 6.2$, $−7.6 ± 5.0$, $−13.0 ± 7.7$ for RC_{max}, RC_{peak}, RC_{mean}, and RC_{vol}. 4DMATCH CTAC recovery was significantly more accurate than 3DMOT, the free-breathing helical CTAC when evaluating RC_{max} ($p = 0.001$), but not significantly more accurate than other CTAC methods or when evaluating other image metrics. When considering only the subset of 4DMATCH images that corresponded to the end-exhale image phase, 4DEXH, mean, and interquartile range were similar to 4DMATCH but variability was considerably reduced.

When evaluating the distribution of recovery coeffecients between RC_{max}, RC_{mean}, RC_{peak}, and RC_{vol} in Kruskal–Wallis ANOVA, significant differences between recovery were found between the different metrics ($p = 0.001$). These trends were characterized by increased variability in the distribution of RC_{vol} recovery and decreased variability with RC_{mean} recovery; however, trends in mean and median recovery were similar between metrics.

3.C. 4DPET recovery as a function of phase

Visual inspection of 4DPET/CT with 4DMATCH reconstruction revealed mismatch between PET and CT images phases (Fig. 6). When testing differences between phases over all CTAC methods and waveforms with Kruskal–Wallis ANOVA, significant differences between phases were revealed ($p = 0.005$). However, these differences were driven by the patient-specific respiratory waveforms; when testing patient and sinusoidal waveforms separately with Kruskal–Wallis ANOVA, patient waveforms were significantly different between phases ($p < 0.0001$) while the sinusoidal waveforms were not significantly different ($p = 0.98$). The 70% and 90% phases, which correspond to the inhale phases where motion is typically greatest in a patient's respiratory cycle, demonstrated poorest accuracy and greatest variability in recovery coefficients (Fig. 7).

3.D. Lesion periphery and threshold sensitivity

The effect of CTAC choice on peripheral enhancement of RC_{max} and RC_{mean} was measured within an isotropic 2 cm expansion of the lesion (Fig. 4). For RC_{max}, a uniform elevation of peripheral uptake for the motion case versus the static case was observed, but no significant differences were measured between CTAC types (Fig. 8). For RC_{mean}, a significant increase in background uptake in the vicinity of the lesion was measured for 4DMIP CTAC versus other CTAC methods on the order of 10% ($p < 0.0001$).

The effect of variance in segmentation threshold on RC_{vol} was also investigated by scaling the threshold obtained from the ground truth comparison of sphere volume. Changes in
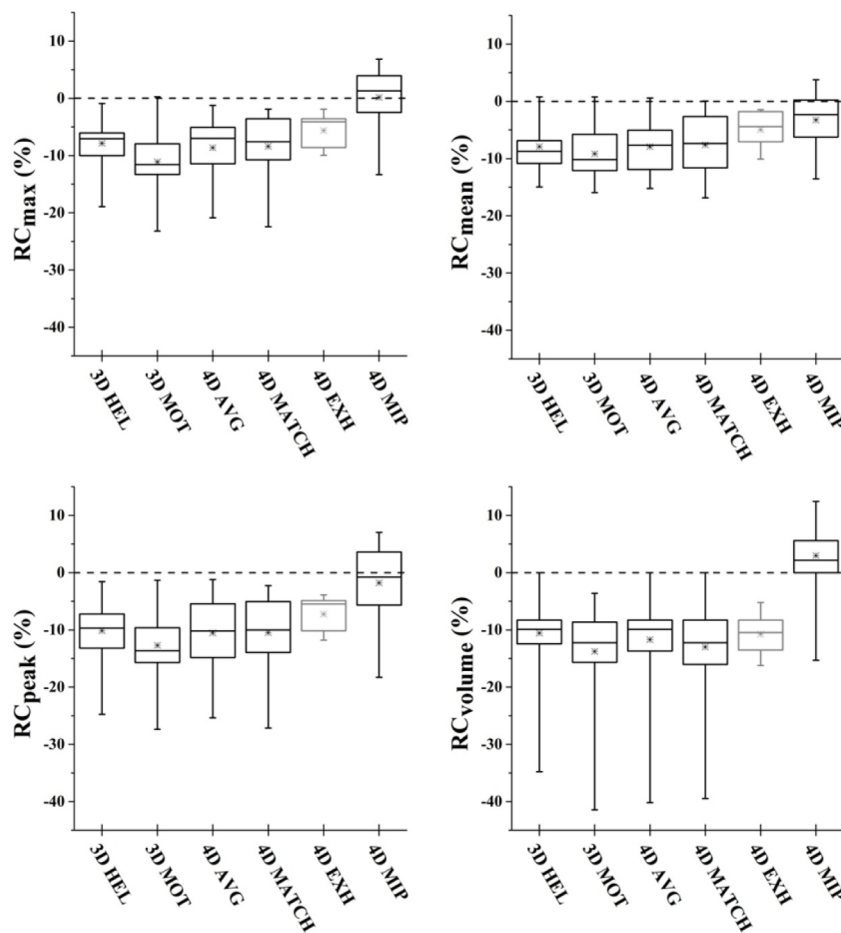
FIG. 5. Box plots depicting 4DPET activity recovery over all investigated respiratory motion waveforms as a function of CTAC. 4DMIP CTAC produced significantly more accurate recovery coefficients. The end-exhale case of 4DEXH demonstrated the least variability; however, note that 4DEXH (depicted in gray) represents only a single PET/CT image phase versus five image phases for the other CTAC methods. Similar trends were seen between metrics. Box represents median and interquartile range of distribution; *x* represents mean; hash marks represent minimum and maximum.

threshold setting led to proportional changes in recovered volume (Fig. 9). For example, recovered volume for 4DMIP was 5.05 ± 0.40 mL for 49.5% of maximum, 5.72 ± 0.33 mL for 45.5%, and 6.45 ± 0.32 mL for 40.5%, while the recovered volume for 4DMATCH was 4.06 ± 0.69 mL for 49.5% of

maximum, 4.83 ± 0.43 mL for 45.5%, and 4.06 ± 0.69 for 40.5%. As a consequence, while 4DMIP demonstrated the highest accuracy of the six methods for thresholds of 45.5% (derived from the ground truth comparison) and 49.5%, it showed lowest accuracy for the 40.5% threshold segmentation.

PET bin	1	2	3	4	5
CT phase	10%	30%	50%	70%	90%
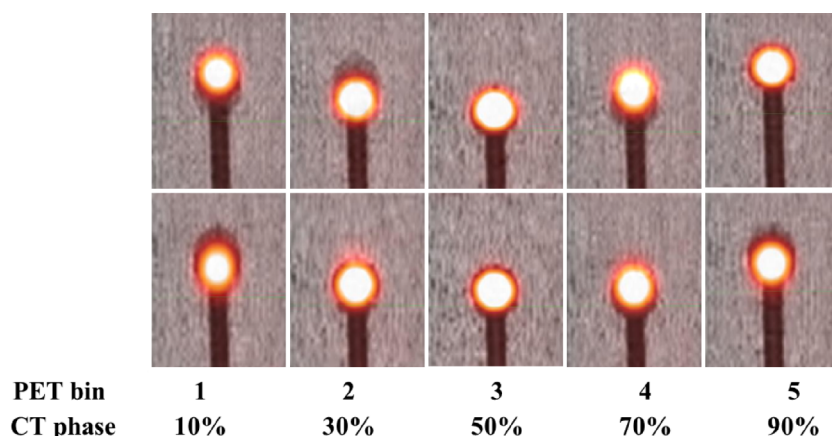
FIG. 6. 4DPET/CT images with phase-matched CT attenuation correction for two representative patient-specific respiratory motion cases. While good agreement is generally seen at end-exhale phases (middle panel), phase mismatch is evident at other phases. CT phase number indicates center of phase bin.
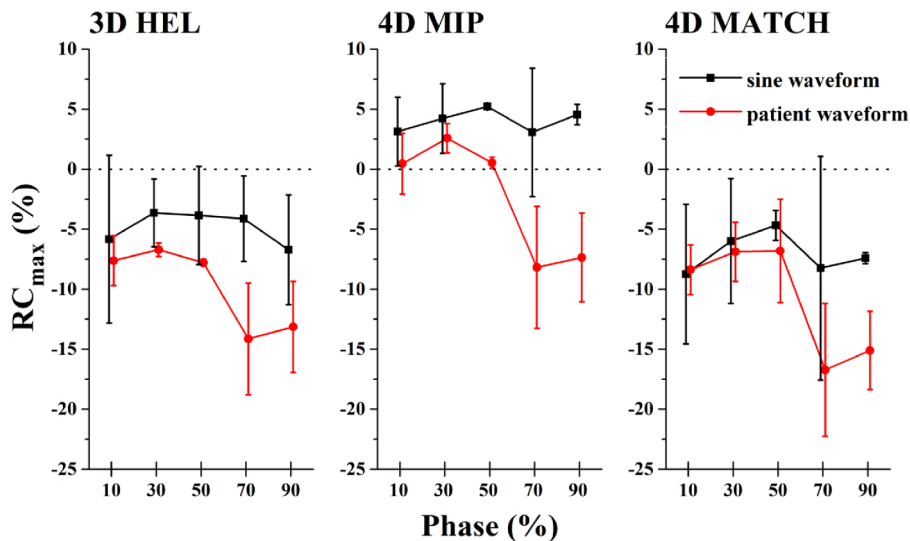
FIG. 7. 4DPET recovery coefficients for maximum uptake as a function of respiratory phase and CTAC method. Patient-specific respiratory waveforms result in reduced accuracy and increased variability versus sinusoidal waveforms in the 70%–90% phase range, which corresponds to inhale phases.

4. DISCUSSION

CT attenuation correction method is an important consideration for thoracic PET quantification in the presence of respiratory motion. In this study, we have investigated the impact of six CTAC methods on PET image quantification in the presence of simulated patient-specific and sinusoidal respiratory motion. In contrast to previously published work, minimal advantage from the use of phase-matched (4DMATCH) CTAC was shown versus other methods such as helical CTAC. Here, strong advantages in accuracy of SUV metrics and thresholded volumes were demonstrated with the use of the maximum intensity projection (4DMIP). These results indicate that though respiratory phase-matched CTAC should in theory provide optimal corrections, image artifacts and differences in implementation of 4DCT and 4DPET sorting can reduce the benefits of this approach.

Despite the theoretical advantages of the phase-matched CTAC method, this study noted significant advantages over other methods in only a single case (significant improvement in RC_{max} compared to helical CTAC in the presence of motion). No significant differences were detected for RC_{peak}, RC_{mean}, or RC_{vol} or versus other CTAC methods. This result for RC_{max} was similarly reported in the literature by Ponisch *et al.*, though their work showed a substantially greater improvement in accuracy, and also an advantage in thresholded volumes, which was not observed here.[26] One distinction between this work and the prior work is the investigation of five motion conditions, including three patient-specific respiratory waveforms. By comparison, the prior work investigated only a single eccentric sinusoidal waveform. The use of patient-specific waveforms is hypothesized to lead to increased CTAC artifacts due to changes in motion patterns over time (Fig. 2). Additionally, the present work used a heterogeneous lung-equivalent background, which leads to more substantial and realistic 4DCT and 4DPET artifacts than the homogeneous background used by the prior work. Killoran *et al.* investigated four sinusoidal waveforms with heterogeneous background
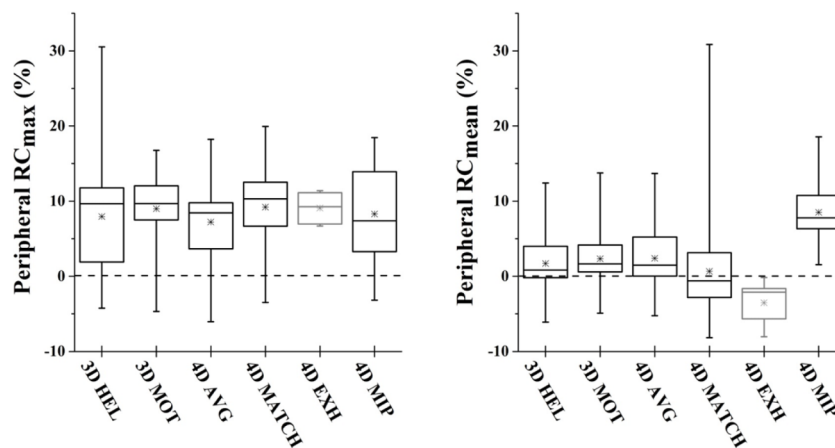
FIG. 8. Effect of CTAC on background enhancement within a 2 cm volumetric expansion of the lesion. No significant differences in maximum uptake were measured. For RC_{mean}, 4DMIP CTAC resulted in higher uptake within the 2 cm expansion on the order of 10%. Box represents median and interquartile range of distribution; x represents mean; hash marks represent minimum and maximum.
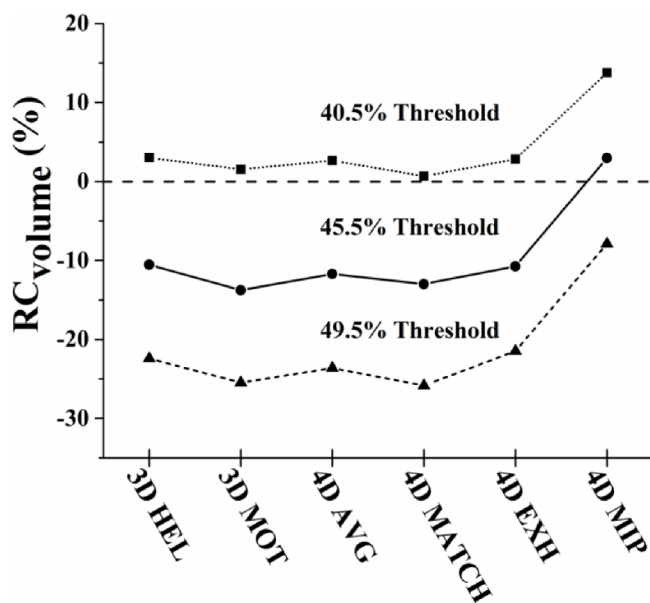
FIG. 9. Volume recovery coefficients as a function of CTAC method and threshold segmentation method. Volume recovery scaled proportionally as a function of percent maximum threshold.

and noted mixed results in comparisons of phase-matched, phase-averaged CTAC, and helical CTAC,[28] which agrees more closely with our results. More investigation is required as differences in experimental design, including design of phantom, respiratory correlation techniques, scanner vendor, commercial or in-house reconstruction software, 2D or 3D PET acquisition, and reconstruction settings will affect image quantification. However, it is clear that 4DPET/CT accuracy is limited by the difference in respiratory sampling during image acquisition: long acquisition time of respiratory-correlated PET integrates motion over many respiratory cycles per phase bin, while the short acquisition time of respiratory-correlated CT integrates motion over only 1–2 respiratory cycles per phase bin, which in turn contributes to phase mismatch of CT and PET images. These effects should be investigated before implementing phase-matched 4DPET workflows for clinical use.

The 4DMIP CTAC showed the highest accuracy in quantitative applications in this phantom study, and has similarly been shown to be advantageous in cardiac PET.[29] However, other factors could lead to reduced accuracy depending upon the application. One concern could be overcorrection at the periphery of the lesion, though the results presented here suggest this is a minor effect. The maximum uptake in the periphery was not increased while the mean uptake in the periphery was elevated on the order of 10%. This suggest modest enhancement of uptake in the voxels closest to the object in motion; however, this enhancement remains below the lesion activity. Furthermore, many of the specific applications of thoracic FDG PET, such as SUV_{max} or SUV_{peak} assessment for treatment response, may be unaffected by minor enhancement in the lesion periphery. Another factor that this experiment is incapable of evaluating is the effect of the maximum intensity projection on the external patient contour, which

may appear larger under respiratory motion and lead to over-correction of photon attenuation and thus uniformly escalated SUV values. Again, for response evaluation, this effect may be reduced in importance assuming general consistency in body habitus and respiration between scans. Despite these limitations, these results motivate further study of the application of the maximum intensity projection CT for thoracic PET/CT attenuation correction.

While the use of a physical respiratory phantom offered the benefit of a controlled experimental design, there are additional limitations with this phantom. Considering that the moving feature was surrounded by lung-equivalent material, the presented results may be specific to PET imaging of lesions in low-density regions. Likewise, the sphere/tumor was filled through a stem that retained modest amounts of residual activity (approximately 10% of the sphere activity) and translated during motion in and out of the tumor position. While this may bias results, the fillable area of the stem is roughly 0.2 cm in diameter compared to the 2.2 cm sphere and should have minimal impact on results. Similarly, the effects of tumor heterogeneity or tracer kinetics in the patient could bias the results versus the uniform sphere used here and cannot be evaluated. Furthermore, we evaluated only a fixed count density and the standard caveats apply that results may vary as a function of lesion-to-background ratio, count density, and noise levels. However, the previous investigation by Park *et al.* of three different tumor-to-background ratios suggests that phantom contrast does not strongly affect 4DPET recovery, and thus the corresponding fractional changes as a function of CTAC method are likely to be small.[27] Counts for 4DPET acquisition were matched to the reference 3DPET acquisition per scan, not per bin, which most closely reflects clinical practice, but could bias the results. However, an analysis of normalizing activities to reference objects defined on 3DPET or 4DPET with corresponding differences in count levels (presented in Appendix) suggests this is not a significant effect.

When considering 4DEXH, which consists of only the end-exhale phase of the 4DMATCH dataset, considerably reduced variability was seen with similar accuracy profiles to 4DMATCH. While accuracy remained lower than 4DMIP, 4DEXH may be an appropriate strategy for response assessment, where reduced variability may be of higher importance than small gains in accuracy, and relative response rates may wash out absolute bias. However, as 4DEXH only represents 20% of the entire respiratory waveform, it would not be appropriate for applications where it is desired to encompass motion, such as radiotherapy target definition in the free-breathing setting.

Limitations of 4DCT image quality in the presence of respiratory motion appeared to be a limiting factor in the performance of various 4DCTAC approaches. Various methods have been proposed to improve robustness and reduce artifacts in respiratory-correlated imaging, including long duration scanning with low dose CT (Ref. 33) and various mathematical approaches such as amplitude-based sorting, deformable interpolation, and respiratory modeling through principle component analysis.[34–36] Similarly, new developments are

underway for 4DPET. The use of linear surrogates such as the camera-based or pressure belt-based systems has been criticized for various reasons, including lack of correlation to tumor motion at depth, and alternative methods under investigation include markerless tracking[37] and full surface tracking.[38]

In this study, we evaluated four common PET image metrics. However, these metrics may not evaluate the impact of attenuation correction methods on other important image characteristics that are used for diagnosis or target definition. As an example, the effect of CTAC on lesion shape, uniformity, heterogeneity, or textural features was not evaluated. Similarly, the limitations of fixed threshold segmentation are well-known, for example, the seminal work of Nestle *et al.*[32] While other advanced segmentation techniques such as adaptive thresholding, gradient methods, or statistical modeling may provide more accurate lesion segmentation,[39–41] the purpose of this study was not to define the optimal segmentation method, but to evaluate the quantitative impact of CTAC choice on threshold segmentation because it is the most commonly used volume metric in the literature. In this study, changes in threshold setting on the order of 10% led to proportional changes in volume recovery, with the magnitude of recovery between CTAC methods remaining roughly constant in proportion to each other. As a result, by reducing the threshold setting below that which was defined from the ground truth comparison, the 4DMIP CTAC showed the poorest accuracy at the 40.5% threshold despite greatest accuracy for all other threshold settings and SUV metrics. This reinforces the challenges of defining an optimal threshold setting outside of a ground truth phantom study, such as for patient data in the clinical setting. Unfortunately, no consensus exists on more optimal segmentation techniques and they are not yet widely available in the clinical environment. Further investigation is warranted on this topic.

5. CONCLUSION

CT attenuation correction method is an important consideration for thoracic PET quantification in the presence of respiratory motion. While respiratory phase-matched CTAC should in theory provide optimal corrections, image artifacts and differences in implementation of 4DCT and 4DPET sorting can degrade the benefit of this approach. Comparative advantages in accuracy and precision of SUV metrics and thresholded volumes were demonstrated with the use of the maximum intensity projection and end-exhale CT attenuation correction. These results may be useful to guide the implementation, analysis, and development of respiratory-correlated thoracic PET/CT in the radiation oncology and diagnostic settings.
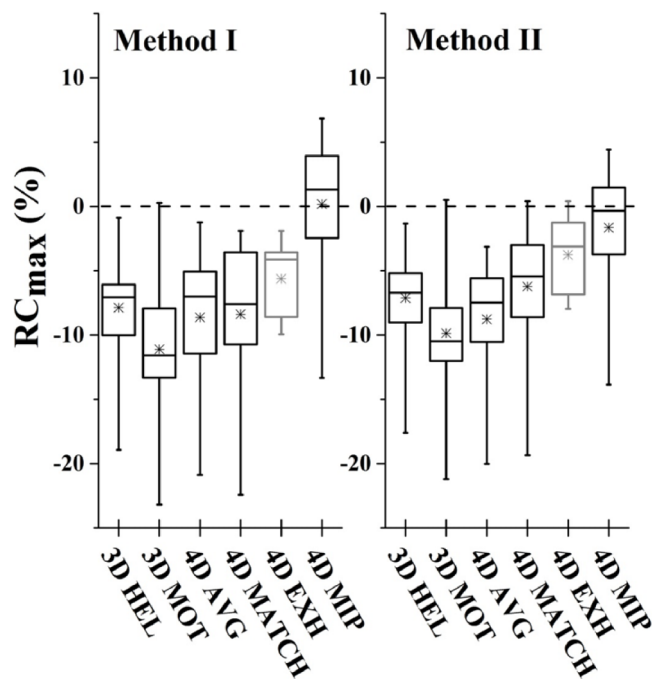
FIG. 10. Comparison of reference method I (ratio of activity in moving 2.2 cm sphere to nonmoving scan) and reference method II (ratio of activity in moving 2.2 cm sphere to 3.7 cm static sphere in same scan). No significant differences were measured between methods.

APPENDIX: COMPARISON OF 3DPET AND 4DPET REFERENCE CONDITIONS

Ratios of recovery for reference method I (normalizing the 2.2 cm sphere in the moving insert to the 2.2 cm sphere under static conditions) and reference method II (normalizing the 2.2 cm sphere in the moving insert to the 3.7 cm sphere in the nonmoving insert) were compared. Since the 4DPET protocol results in 20% of the total number of counts in any given image phase relative to the 3DPET reference case, it can be hypothesized that increased noise in individual phases could lead to differences in results for metrics such as RC_{max}. However, no significant differences were found between the two methods (Fig. 10).

a)Author to whom correspondence should be addressed. Electronic mail: nyflot@uw.edu; Telephone: (206) 598-4100.

[1]U. Nestle, K. Walter, S. Schmidt, N. Licht, C. Nieder, B. Motaref, D. Hellwig, M. Niewald, D. Ukena, C. M. Kirsch, G. W. Sybrecht, and K. Schnabel, "18F-deoxyglucose positron emission tomography (FDG-PET) for the planning of radiotherapy in lung cancer: High impact in patients with atelectasis," Int. J. Radiat. Oncol., Biol., Phys. **44**, 593–597 (1999).

[2]J. F. Vansteenkiste, S. G. Stroobants, P. R. De Leyn, P. J. Dupont, J. Bogaert, A. Maes, G. J. Deneffe, K. L. Nackaerts, J. A. Verschakelen, T. E. Lerut, L. A. Mortelmans, and M. G. Demedts, "Lymph node staging in non-small-cell lung cancer with FDG-PET scan: A prospective study on 690 lymph node stations from 68 patients," J. Clin. Oncol. **16**, 2142–2149 (1998).

[3]L. J. Vanuytsel, J. F. Vansteenkiste, S. G. Stroobants, P. R. De Leyn, W. De Wever, E. K. Verbeken, G. G. Gatti, D. P. Huyskens, and G. J. Kutcher, "The impact of (18)F-fluoro-2-deoxy-D-glucose positron emission tomography (FDG-PET) lymph node staging on the radiation treatment volumes in patients with non-small cell lung cancer," Radiother. Oncol. **55**, 317–324 (2000).

[4]J. Bradley, W. L. Thorstad, S. Mutic, T. R. Miller, F. Dehdashti, B. A. Siegel, W. Bosch, and R. J. Bertrand, "Impact of FDG-PET on radiation therapy

volume delineation in non-small-cell lung cancer," Int. J. Radiat. Oncol., Biol., Phys. **59**, 78–86 (2004).

[5]J. Bradley, K. Bae, N. Choi, K. Forster, B. A. Siegel, J. Brunetti, J. Purdy, S. Faria, T. Vu, W. Thorstad, and H. Choy, "A phase II comparative study of gross tumor volume definition with or without PET/CT fusion in dosimetric planning for non-small-cell lung cancer (NSCLC): Primary analysis of radiation therapy oncology group (RTOG) 0515," Int. J. Radiat. Oncol., Biol., Phys. **82**, 435–441.e1 (2012).

[6]J. L. Fox, R. Rengan, W. O'Meara, E. Yorke, Y. Erdi, S. Nehmeh, S. A. Leibel, and K. E. Rosenzweig, "Does registration of PET and planning CT images decrease interobserver and intraobserver variation in delineating tumor volumes for non-small-cell lung cancer?," Int. J. Radiat. Oncol., Biol., Phys. **62**, 70–75 (2005).

[7]C. B. Caldwell, K. Mah, Y. C. Ung, C. E. Danjoux, J. M. Balogh, S. N. Ganguli, and L. E. Ehrlich, "Observer variation in contouring gross tumor volume in patients with poorly defined non-small-cell lung tumors on CT: The impact of 18FDG-hybrid PET fusion," Int. J. Radiat. Oncol., Biol., Phys. **51**, 923–931 (2001).

[8]E. A. Usmanij, L. F. de Geus-Oei, E. G. Troost, L. Peters-Bax, E. H. van der Heijden, J. H. Kaanders, W. J. Oyen, O. C. Schuurbiers, and J. Bussink, "18F-FDG PET early response evaluation of locally advanced non-small cell lung cancer treated with concomitant chemoradiotherapy," J. Nucl. Med. **54**, 1528–1534 (2013).

[9]M. Massaccesi, M. L. Calcagni, M. G. Spitilli, F. Cocciolillo, F. Pelligro, L. Bonomo, V. Valentini, and A. Giordano, "18F-FDG PET-CT during chemoradiotherapy in patients with non-small cell lung cancer: The early metabolic response correlates with the delivered radiation dose," Radiat. Oncol. **7**, 106 (2012).

[10]W. Huang, T. Zhou, L. Ma, H. Sun, H. Gong, J. Wang, J. Yu, and B. Li, "Standard uptake value and metabolic tumor volume of 18F-FDG PET/CT predict short-term outcome early in the course of chemoradiotherapy in advanced non-small cell lung cancer," Eur. J. Nucl. Med. Mol. Imaging **38**, 1628–1635 (2011).

[11]W. van Elmpt, D. De Ruysscher, A. van der Salm, A. Lakeman, J. van der Stoep, D. Emans, E. Damen, M. Ollers, J. J. Sonke, and J. Belderbos, "The PET-boost randomised phase II dose-escalation trial in non-small cell lung cancer," Radiother. Oncol. **104**, 67–71 (2012).

[12]H. J. Aerts, A. A. van Baardwijk, S. F. Petit, C. Offermann, J. Loon, R. Houben, A. M. Dingemans, R. Wanders, L. Boersma, J. Borger, G. Bootsma, W. Geraedts, C. Pitz, J. Simons, B. G. Wouters, M. Oellers, P. Lambin, G. Bosmans, A. L. Dekker, D. De, and Ruysscher, "Identification of residual metabolic-active areas within individual NSCLC tumours using a pretreatment (18)Fluorodeoxyglucose-PET-CT scan," Radiother. Oncol. **91**, 386–392 (2009).

[13]C. Cohade, M. Osman, L. N. Marshall, and R. N. Wahl, "PET-CT: Accuracy of PET and CT spatial registration of lung lesions," Eur. J. Nucl. Med. Mol. Imaging **30**, 721–726 (2003).

[14]Y. E. Erdi, S. A. Nehmeh, T. Pan, A. Pevsner, K. E. Rosenzweig, G. Mageras, E. D. Yorke, H. Schoder, W. Hsiao, O. D. Squire, P. Vernon, J. B. Ashman, H. Mostafavi, S. M. Larson, and J. L. Humm, "The CT motion quantitation of lung lesions and its impact on PET-measured SUVs," J. Nucl. Med. **45**, 1287–1292 (2004).

[15]G. W. Goerres, E. Kamel, B. Seifert, C. Burger, A. Buck, T. F. Hany, and G. K. Von Schulthess, "Accuracy of image coregistration of pulmonary lesions in patients with non-small cell lung cancer using an integrated PET/CT system," J. Nucl. Med. **43**, 1469–1475 (2002).

[16]P. E. Kinahan, B. H. Hasegawa, and T. Beyer, "X-ray-based attenuation correction for positron emission tomography/computed tomography scanners," Semin. Nucl. Med. **33**, 166–179 (2003).

[17]C. Liu, L. A. Pierce II., A. M. Alessio, and P. E. Kinahan, "The impact of respiratory motion on tumor quantification and delineation in static PET/CT imaging," Phys. Med. Biol. **54**, 7345–7362 (2009).

[18]T. Pan, O. Mawlawi, S. A. Nehmeh, Y. E. Erdi, D. Luo, H. H. Liu, R. Castillo, R. Mohan, Z. Liao, and H. A. Macapinlac, "Attenuation correction of PET images with respiration-averaged CT images in PET/CT," J. Nucl. Med. **46**, 1481–1487 (2005).

[19]T. Beyer, G. Antoch, T. Blodgett, L. F. Freudenberg, T. Akhurst, and S. Mueller, "Dual-modality PET/CT imaging: The effect of respiratory motion on combined image quality in clinical oncology," Eur. J. Nucl. Med. Mol. Imaging **30**, 588–596 (2003).

[20]S. A. Nehmeh, Y. E. Erdi, C. C. Ling, K. E. Rosenzweig, H. Schoder, S. M. Larson, H. A. Macapinlac, O. D. Squire, and J. L. Humm, "Effect of

respiratory gating on quantifying PET images of lung cancer," J. Nucl. Med. **43**, 876–881 (2002).

[21]E. C. Ford, G. S. Mageras, E. Yorke, and C. C. Ling, "Respiration-correlated spiral CT: A method of measuring respiratory-induced anatomic motion for radiation treatment planning," Med. Phys. **30**, 88–97 (2003).

[22]S. S. Vedam, P. J. Keall, V. R. Kini, H. Mostafavi, H. P. Shukla, and R. Mohan, "Acquiring a four-dimensional computed tomography dataset using an external respiratory signal," Phys. Med. Biol. **48**, 45–62 (2003).

[23]D. A. Low, M. Nystrom, E. Kalinin, P. Parikh, J. F. Dempsey, J. D. Bradley, S. Mutic, S. H. Wahab, T. Islam, G. Christensen, D. G. Politte, and B. R. Whiting, "A method for the reconstruction of four-dimensional synchronized CT scans acquired during free breathing," Med. Phys. **30**, 1254–1263 (2003).

[24]T. Pan, T. Y. Lee, E. Rietzel, and G. T. Chen, "4D-CT imaging of a volume influenced by respiratory motion on multi-slice CT," Med. Phys. **31**, 333–340 (2004).

[25]C. C. Nagel, G. Bosmans, A. L. Dekker, M. C. Ollers, D. K. De Ruysscher, P. Lambin, A. W. Minken, N. Lang, and K. P. Schafers, "Phased attenuation correction in respiration correlated computed tomography/positron emitted tomography," Med. Phys. **33**, 1840–1847 (2006).

[26]F. Ponisch, C. Richter, U. Just, and W. Enghardt, "Attenuation correction of four dimensional (4D) PET using phase-correlated 4D-computed tomography," Phys. Med. Biol. **53**, N259–N268 (2008).

[27]S. J. Park, D. Ionascu, J. Killoran, M. Mamede, V. H. Gerbaudo, L. Chin, and R. Berbeco, "Evaluation of the combined effects of target size, respiratory motion and background activity on 3D and 4D PET/CT images," Phys. Med. Biol. **53**, 3661–3679 (2008).

[28]J. H. Killoran, V. H. Gerbaudo, M. Mamede, D. Ionascu, S. J. Park, and R. Berbeco, "Motion artifacts occurring at the lung/diaphragm interface using 4D CT attenuation correction of 4D PET scans," J. Appl. Clin. Med. Phys. **12**, 261–274 (2011).

[29]A. M. Alessio, S. Kohlmyer, K. Branch, G. Chen, J. Caldwell, and P. Kinahan, "Cine CT for attenuation correction in cardiac PET/CT," J. Nucl. Med. **48**, 794–801 (2007).

[30]R. L. Wahl, H. Jacene, Y. Kasamon, and M. A. Lodge, "From RECIST to PERCIST: Evolving considerations for PET response criteria in solid tumors," J. Nucl. Med. **50**(Suppl. 1), 122S–150S (2009).

[31]Y. E. Erdi, O. Mawlawi, S. M. Larson, M. Imbriaco, H. Yeung, R. Finn, and J. L. Humm, "Segmentation of lung lesion volume by adaptive positron emission tomography image thresholding," Cancer **80**, 2505–2509 (1997).

[32]U. Nestle, S. Kremp, A. Schaefer-Schuler, C. Sebastian-Welsch, D. Hellwig, C. Rube, and C.-M. Kirsch, "Comparison of different methods for delineation of 18F-FDG PET-positive tissue for target volume definition in radiotherapy of patients with non-small cell lung cancer," J. Nucl. Med. **46**, 1342–1348 (2005).

[33]T. Xia, A. M. Alessio, B. De Man, R. Manjeshwar, E. Asma, and P. E. Kinahan, "Ultra-low dose CT attenuation correction for PET/CT," Phys. Med. Biol. **57**, 309–328 (2012).

[34]J. Ehrhardt, R. Werner, D. Saring, T. Frenzel, W. Lu, D. Low, and H. Handels, "An optical flow based method for improved reconstruction of 4D CT data sets acquired during free breathing," Med. Phys. **34**, 711–721 (2007).

[35]N. Wink, C. Panknin, and T. D. Solberg, "Phase versus amplitude sorting of 4D-CT data," J. Appl. Clin. Med. Phys. **7**, 77–85 (2006).

[36]Q. Zhang, A. Pevsner, A. Hertanto, Y. C. Hu, K. E. Rosenzweig, C. C. Ling, and G. S. Mageras, "A patient-specific respiratory model of anatomical motion for radiation treatment planning," Med. Phys. **34**, 4772–4781 (2007).

[37]P. J. Schleyer, M. J. O'Doherty, S. F. Barrington, and P. K. Marsden, "Retrospective data-driven respiratory gating for PET/CT," Phys. Med. Biol. **54**, 1935–1950 (2009).

[38]H. Fayad, T. Pan, O. Pradier, and D. Visvikis, "Patient specific respiratory motion modeling using a 3D patient's external surface," Med. Phys. **39**, 3386–3395 (2012).

[39]H. Li, W. L. Thorstad, K. J. Biehl, R. Laforest, Y. Su, K. I. Shoghi, E. D. Donnelly, D. A. Low, and W. Lu, "A novel PET tumor delineation method based on adaptive region-growing and dual-front active contours," Med. Phys. **35**, 3711–3721 (2008).

[40]M. Hatt, C. Cheze le Rest, A. Turzo, C. Roux, and D. Visvikis, "A fuzzy locally adaptive Bayesian segmentation approach for volume determination in PET," IEEE Trans. Med. Imaging **28**, 881–893 (2009).

[41]X. Geets, J. A. Lee, A. Bol, M. Lonneux, and V. Gregoire, "A gradient-based method for segmenting FDG-PET images: Methodology and validation," Eur. J. Nucl. Med. Mol. Imaging **34**, 1427–1438 (2007).